Non-Destructive Investigation of Thermoplastic Reinforced Composites

Ahmed Arabi Hassen[1, 2 PhD and corresponding author]

[1]Manufacturing Demonstration Facility, Oak Ridge National Laboratory, Knoxville, TN, USA
NTRC II, 2360 Cherahala Blvd, Knoxville, TN, 37932, email: hassenaa@ornl.gov, Tel: +1 (205) 470-4010

[2]Department of Materials Science and Engineering, Materials Processing & Applications Development (MPAD) Center, University of Alabama at Birmingham, Birmingham, AL, USA
Business Engineering Complex (BEC), 1150 10th Avenue South – BEC 254, Birmingham, AL, 35294-4461

Hossein Taheri[3 doctoral student]

Department of Mechanical Engineering & Center for Nondestructive Evaluation, Iowa State University, Ames, IA, USA
email: htaheri@iastate.edu

Uday K. Vaidya[4 professor]

Department of Mechanical, Aerospace and Biomedical Engineering, University of Tennessee, Knoxville, TN, USA
email: uvaidya@utk.edu

* THIS MANUSCRIPT HAS BEEN AUTHORED BY UT-BATTELLE, LLC UNDER CONTRACT NO. DE-AC05-00OR22725 WITH THE U.S. DEPARTMENT OF ENERGY. THE UNITED STATES GOVERNMENT RETAINS AND THE PUBLISHER, BY ACCEPTING THE ARTICLE FOR PUBLICATION, ACKNOWLEDGES THAT THE UNITED STATES GOVERNMENT RETAINS A NON-EXCLUSIVE, PAID-UP, IRREVOCABLE, WORLD-WIDE LICENSE TO PUBLISH OR REPRODUCE THE PUBLISHED FORM OF THIS MANUSCRIPT, OR ALLOW OTHERS TO DO SO, FOR UNITED STATES GOVERNMENT PURPOSES. THE DEPARTMENT OF ENERGY WILL PROVIDE PUBLIC ACCESS TO THESE RESULTS OF FEDERALLY SPONSORED RESEARCH IN ACCORDANCE WITH THE DOE PUBLIC ACCESS PLAN (HTTP://ENERGY.GOV/DOWNLOADS/DOE-PUBLIC-ACCESS-PLAN).

ABSTRACT

This paper studies various manufacturing defects in glass fiber / Polypropylene (PP) composite parts and their methods of detection. Foreign Object Inclusion (FOI) of different shapes, sizes, and materials were placed in a glass fiber / PP panel made by compression molding. The paper aims to characterize the fiber orientation and fiber related defects such as fiber waviness in the composite specimen. Comprehensive investigation for different Non Destructive Evaluation (NDE) techniques, namely X-ray radiography and

© 2016. This manuscript version is made available under the Elsevier user license
http://www.elsevier.com/open-access/userlicense/1.0/

Ultrasonic Testing (UT) techniques to trace and characterize the embedded defects and the composite texture are presented. Conventional X-ray radiography successfully identified the fiber orientation in two dimension (2-D) plane; however, information for the sample depth was not captured. The radiography techniques showed low relative errors for the defect size measurements (maximum error was below 9.5%) when compared to the ultrasonic techniques. Ultrasonic techniques were able to map all the embedded artificial defects. Phase Array (PA) ultrasonic technique was able to precisely locate the FOI in the glass fiber / PP specimen. Nerveless, the shape and size of the defects were not accurately determined due to the high signal attenuation and distortion characteristics of the E-glass fiber.

Key words: A. Thermoplastic resin; A. Glass fibers; B. Defects; D. Non-destructive testing; E. Compression moulding

1. INTRODUCTION

Composite material applications have grown rapidly over the last few years as market studies showed that the US composite market grew by 6.3 percent to reach $8.2 billion in 2014 and the main economic indicators predicts a growth of 4.9 percent by the end of 2015 [1]. The market study shows that glass fiber is the most dominant material in the reinforcement segment [1]. This market expansion is due to the superior composite materials properties (i.e. high strength to weight ratio, corrosion resistance, high specific modulus and their improved damping capacity) [2, 3]. Thermoplastic reinforced composite materials are widely used in the fabrication of various high-end products in many industrial applications such as marine and offshore, mass-transit and automotive industry [4, 5]. They are being preferred over other composite materials as they have a shorter processing times and the ability to being recycled [6, 7]. Different discontinuity mechanisms can occur during the manufacturing processes or at the service life of the component. Defects such as fiber wrinkling and waviness, porosity, FOI, and ply misalignment that can progress during the fabrication process could lead to other damages such as delamination, disband, and crack formation [8-10]. The characterization of these defects is extremely important and it is preferable to be evaluated nondestructively. With the increase of the composite share the efforts for Non Destructively

Evaluation / Testing (NDE/T) are exploding and over the past few years various NDE techniques have gradually percolated into mainstream testing criteria on a global scale.

Several NDT/E techniques such as X-ray, thermography, ultrasonic testing and techniques are widely used to characterize different defects in composite materials [11-13]. Thermography could be used to study near surface regions of composite structure [11]. This technique mainly detects near surface features. However, it can penetrate a shallow depth through the material (few millimeters) depends on the modulation frequency and the type of material tested. The technique suffers from depth limitation, as the attenuation of the modulated thermal diffusion process is high [14]. Radiography is widely used in defect and discontinuity detection in composite materials [15, 16]. However, special considerations should be taken when scanning low atomic weight elements (such as polymers) with low X-ray attenuation coefficients. Low energy X-ray parameters (i.e. tube voltage of an average between 10 and 50 keV) with short exposure time are often used to test polymeric materials [17, 18]. Conventional X-ray radiography suffers from structural superposition (i.e. lack of providing three dimension (3-D) information). On the other hand, X-ray CT technique provides 2-D density maps of the part cross sections that can be stacked together to provide accurate 3-D information of the entire part. Researchers used X-ray CT to detect several types of discontinuities and characterize different composite materials and structures, including honeycomb composites, fiberglass power poles, and carbon foams [19-21].

UT is a widely used technique for internal defects detection in composite materials, quality inspection, control and monitoring for different applications such as wind turbine blades, ship hulls, automotive components, aircraft structures piping and welds [18, 22-24]. Using A-scan ultrasonic inspection technique for detecting defects in composite is quite challenging, however the interpretation of the scanned signals could provide indications for the location and the depth of the defects, accurate information about the shape and the size of the defect is difficult to be visualized [25]. C-scan mapping technology offer a standard, easy defect detection and more detailed evaluation compared to intensive manual scanning of conventional methods. Theodoros et al. characterized two different types of materials used for marine applications (i.e. carbon/epoxy and glass/polyester) using C-scan UT [26]. Both were fabricated using 14 laminates where several artificial defects were embedded into the test plates. Using a flat UT transducer, they were able to

determine the location and the shape of the defects. However, in some cases the exact size was difficult to be obtained. Fiber waviness is a material defect that occurs at the fabrication stage and can be divided into out-of-plane and in-plane fiber waviness [27]. Fiber waviness could result in a substantial decrease in the mechanical properties as the fiber shear angle increased, hence it is curtail to identify and detect the areas of fiber waviness in the fabricated composite part. Research work done in the measurement of in-plane and out-of-plane fiber waviness using ultrasonic testing can be found in [10, 27, 28]. Dayal successfully developed a theoretical model of a longitudinal wave propagating through a composite laminate with a wavy sublamina [10]. The wavy lamina was buried inside the composite laminate and is not visible from the outside. He validated his model experimentally using a set of graphite/epoxy wavy laminates.

In previous research we attempted to study artificial defects embedded in a thick glass fiber / PP composite (i.e. 80 plies with overall thickness of ≈ 14.1 mm) with high fiber loading of 80% by weight using UT C-scan system [8]. Conventional flat transducer with two different frequencies (i.e. 5 MHz and 2.25 MHz) were used to scan the specimen and it was found that most of the defects were not detected due to the high signal attenuation characteristic of the E-glass fibers. This could be overcome using lower frequency (i.e. 1 MHz) through transmission ultrasonic or PA ultrasonic system. PA UT has the ability to inspect large structures quickly and can be customized for individual applications [29]. In contrast to conventional flat transducers, where a single-element probe is used, PA transducers uses multi-element probes in which each individual element can transmit and receive ultrasonic signals independently at different times. In this technique time delay is set for individual element to generate interference of the ultrasonic wave fronts that allows the energy to be focused and steered at any specified depth and angle in the test sample. Ber et al. were able to detect different size defects (ranging from less than 6.35 mm to inches to 19 mm) in a composite tube using a curved PA props. They only reported qualitatively that the defects were clearly visible in the time-of-flight and amplitude C-scans [30]. The work presented in this paper aims to study the capabilities and limitation of radiography method and ultrasonic techniques when used to detect fiber orientation, fiber waviness and FOI in thermoplastic composites. The effect of changing the inspection technique parameters and configurations on the ability of quantitatively characterizing the FOI defects shape and size is within the interest of this paper.

2. MATERIALS AND TEST SPECIMENS PREPARATION

Thermoplastic composite, namely glass fiber / PP, was used to fabricate the specimen used in this work. The glass fiber / PP was provided by (Polystrand Inc.) in a tape form with density of 1.9 g/cm^3 and 80% as glass fiber weight fraction. The specimen were fabricated using a total of 80 plies with X-ply $[0/90]_{80}$ configuration and with dimensions of 152.4 mm (6 inch) x 152.4 mm (6 inch) and cross-sectional thickness of approximately 14.1 mm (0.55 inch) and total weight of 630 g. The plies were stacked and molded into squared shape plaque using 150 metric ton press (Pasadena Hydraulic Inc.). The tool was heated up to 170.5^{o}C (339 F) in a constant rate of 5^{o}C/min. As the temperature reached 65.5^{o}C (150 F), 10 tons of pressure was applied. The dwell time was 40 minutes and then allowed to cool in air.

Six artificial defects with different shapes and materials were embedded in the panel to help assess the capabilities of the inspection system and criteria limits, as shown Figure 1. The dimensions and the locations for the defects are listed in Table 1 and Figure 1. The selections of the distances between the defects were carefully designed to avoid interference between each defect and its neighbor during the inspection process. The A1, A2 and A4 FOI are made from Kapton and Teflon as shown in Table 1 that has densities comparable to the Glass Fiber Reinforced Plastic (GFRP) composite density (≈ 2.1 g/cm^3 and 1.4 g/cm^3 for Teflon and Kapton respectively). These types of FOI are presented to evaluate the NDT/E systems capabilities to distinguish these FOI from the background material. A3 and A5 are metallic FOI with relatively larger thickness, compared to the other FOI. The insert of A3 and A5 FOI into the composite laminates will create a separation between the adjacent plies at two different locations shown in Figure 1. The A6 defect was created by oversize cut, relative to the compression-molding mold, of the last 12 plies that created fiber waviness defect during the compression molding process.

3. EXPERIMENTAL SETUP

Two different NDT techniques were used in this study, namely ultrasonic testing and radiography. The UT method is divided into two categories: Phase Array UT and Through Transmission UT (TT UT). In radiography, two different methods were used in this work: X-ray radiography and X-ray CT. Moreover, two different X-ray imaging procedures were used for imaging the samples that include convention focusing (i.e.

macro focus) and micro focus, which are described in more detail in later sections.

3.1 X-RAY SYSTEMS

3.1.1 X-Ray Radiography

North Star Imaging (NSI) M5000 X-ray system was used for real time imaging of the samples. It has the capability for both macro and micro focus tube that allows detection for the discontinuities at various resolutions and sizes. Figure 2 shows the X-ray imaging setup for the glass fiber/PP plate. The sample was mounted on the positioning system's table in between the detector and the tube and lined up in the holding supports. The test parameters were optimized for the best imaging results, a voltage and currents 75 kV and 250 mA respectively were applied. Display-Field-of-View (DFOV) of 180 mm and scan resolution of 200 μm.

3.1.2 X-ray CT-scan

A helical scanning mode was used to scan the composite specimen using GE Discover 750 HD CT-scanner with current of 200 mA, energy of 80 kV, DFOV of 200 mm and scan resolution of 350 μm. 2-D density images of cross sections through the specimen were acquired through tomographic reconstruction and Multi Planer Reconstruction (MPR) method was used to visualize the volumetric data. The segmentation and visualization of the volumetric data set were carried using Osirix imaging software [31].

3.2 ULTRASONIC TESTING

3.2.1 Phase Array Ultrasonic

A 64 element phase array transducer with 2.25 MHz frequencies were used to scan the glass fiber / PP specimen. A zero degree (SA2-0L) wedge was used to couple the sound energy and to protect the transducer face from abrasion during the scan. The data were acquired through Olympus (OmniScan MX2) transmitting-receiving system and one line encoder was used to track the transducer position while scanning the specimen. Primarily, only 32 elements with a gain of 26 dB were used and the signal was focused at the specimen back wall. The gate was placed at the back wall signal and maximum peak strategy was used to

identify all the defects at the specimen. Subsequently, B-scan and C-scan data for the full specimen area were obtained and analyzed. Accordingly the ultrasonic beam was steered and focused at each individual FOI (i.e. the beam were focused at different depth through the specimen thickness) to enhance the detectability of the defects.

3.2.2 Through Transmission Ultrasonics

AG-2 overhead 10 Axis gantry scanner squirted system, designed and manufactured by Marietta NDT, Georgia, USA, was used to scan the samples as shown in Figure 3. The water forced through nozzles with 3.1 mm (0.125 inch) diameter to aid the ultrasonic beam to travel through a narrow water bath to the specimen surface. TT UT transducers were used to scan the specimen with a frequency of 1 MHz. The transducer was a focused transducer with element dimensions of 38.1 mm (1.5 inch) and 23.9 mm (0.94 inch) as outer diameter inner diameter respectively. A scanning speed of 200 mm/s (7.8 inch/s) with a resolution of 0.5 mm (0.019 inch) and an overall gain of 40 dB was used and Olympus MultiScan MS5800 scan 8 channel system were used to acquire the data.

4. RESULTS

4.1 X-RAY RADIOGRAPHY

4.1.1 Conventional X-ray

Figure 4 shows a 2-D density image for the glass fiber / PP specimen acquired using X-ray system. The density is correlated to the point-by-point linear attenuation coefficient using the following relation [32]:

$$\int \mu\,(s)\,ds = -\ln\left(\frac{I}{I_0}\right) \quad (1)$$

where, I_0 is the intensity of the un-attenuated radiation, I is the intensity of the attenuated radiation over the integrated path length and μ is the linear attenuation coefficient. The attenuation coefficient is correlated to the contrast through [33],

$$\text{Contrast} = \frac{|\mu_O - \mu_B|}{\mu_B} \times 100 \quad (2)$$

where, μ_O is the attenuation coefficient of the object of interest and μ_B is the attenuation coefficient for the

background material. From Figure 4 it was observed that only FOI A3 and A5 (i.e. Steel and Aluminum plate respectively) were detectable as they have a higher contrast difference between the FOI material and the background material. However, A2 and A4 (i.e. made out of Teflon) were not detected and this is attributed to the insufficient density changes between Teflon inserts (density ≈ 2.1 g/cm^3) and the GFRP (density ≈ 1.9 g/cm^3) that results in low contrast between the defects and background material [34, 35].

In contrast to the Teflon insert, Kapton insert has relatively higher density difference (density ≈ 1.4 g/cm^3). However, it was noticed that the conventional X-ray system was not able to detect the Kapton insert. In order to reveal more details, high resolution X-ray source was used (i.e. micro focus) to detect the Kapton insert, as shown in Figure 4b. The results showed that the Kapton insert is still undetectable. Figure 4 shows the fiber 0º/90º orientation pattern in the specimen due to the density difference between the glass fibers (density ≈ 2.58 g/cm^3) and the PP matrix (density ≈ 0.91 g/cm^3) [36]. However, fiber waviness (i.e. A6 defect) was not identified, as the final X-ray image is a structural superposition of all layers perpendicular to the scanning direction.

4.1.2 X-ray CT-scan

Figure 5a shows X-ray CT volumetric data displayed as 3-D solid object for the glass fiber / PP specimen. The 3-D reconstruction was virtually sectioned using a cutting plane (i.e. A-A) orthogonal to the cross-sectional image plane and at different depth measured from the top surface of the specimen, as shown in Figure 5b-e. This maps the X-ray density values on the sectioned plane and shows the FOI location across the specimen thickness. Figure 5b shows the fiber waviness (defect A6) that resulted from the oversize cut of the plies 68 to 80. Figure 5c and Figure 5d show a clear representation for Aluminum plate and circular steel plate inserts. Unlike the conventional X-ray system, CT scanning method detected the Kapton insert. However, it was observed that the contrast differences between the Kapton insert and the background material is low as shown in Figure 5e.

It was noticed from Figure 5 that the metallic inserts produce artifacts (i.e. dark streaks between metallic object and surrounded by bright streaks). This type of artifact is associated with high atomic number metals and is generated due to beam hardening. High atomic number objects tend to have high attenuation for

lower X-ray energy. The attenuation of the low energy X-ray photons is easier than the attenuation of high-energy photons and is proportional to Z^3/E^3, where Z is the atomic number and E is the X-ray energy [37]. Beam hardening for high attenuate material results in the detection of larger number of photons that results in these artifacts (i.e. streaks). This type of artifact can be compensated using higher scanning kV that produces harder X-ray beam. Nevertheless, the scanning contrast is compromised (i.e. objects with similar X-ray attenuation coefficient (in this case Kapton and Teflon)) will not be distinguished. Several reconstructing techniques have been developed to reduce the effect of the metal artifact [37, 38]. It should be noticed that these reconstruction techniques would resolve the artifact problem; however, decrease in the resolution would take place.

4.2 ULTRASONIC TESTING

Attenuation of sound in a medium occurs as a combination effect of scattering and absorption. As the sound travels through a material, the intensity of the sound reduces over the distance. A contact pulse echo method was used to determine ultrasonic attenuation characteristics in glass fiber / PP specimen used in this research. Wide band ultrasonic transducers with the central frequency 0.5 MHz, 1 MHz, 2 MHz, 2.25 MHz and 5.0 MHz were used for the measurements. This investigation will assist in selecting the desired frequency to scan glass fiber/ PP specimen with any given thickness. Figure 6 shows a relation between the material attenuation and the frequency. It was noticed that the attenuation of the sound wave strongly depends on the frequency. The signal attenuation that corresponds to the 2.25 MHz and 1 MHz frequency has an average value of 2.5 dB/mm and 2 dB/mm respectively. This delivers a clear indication that using high frequency will result in insufficient results while scanning thick glass fiber / PP composite (~ 14.1 mm) with high fiber loading (~ 80 % by weight) used in this research.

4.2.1 Phase Array Ultrasonic

Because of the multi element signal focusing, PA UT shows better characteristics of attenuation and resolution of the ultrasonic signals. Figure 7 presents amplitude C-scan PA UT results for the glass fiber / PP specimen at scanning frequency of 2.25MHz. The gate was placed at back wall echo and the maximum peak

strategy was used in order to define the FOI on the specimen. The FOI are presented in Figure 7 with different colors (i.e. red color represent highest amplitude > 80 dB). Figure 7a shows C-scan mapping for the defects location and shape while Figure 7b is B-scan map showing the FOI location across the sample depth. It was observed that the technique identified the location of the defects accurately. However, the shape of the defects was not precisely identified. This is attributed to two main reasons. First is the high signal attenuation characteristic of glass fiber, and the second is the FOI create ply separation and delamination at the adjacent areas, which results in signal distortion. The amplitude of the FOI at these areas are mixed with echoes coming from the delaminated areas which result in echoes that are recognized as FOI area. Consequently, the UT signal was steered and focused at different depths in the samples (i.e. equivalent to the defects location across the specimen thickness), in an attempt to enhance the identification of the defect shape. Areas of amplitude of ~ 60 dB were observed at different locations in the specimen and it has higher concentrations near to the top surface of the specimen as shown in Figure 7 (pointed as II). These areas (pointed as II) are an evidence for the presence of fiber waviness (i.e. A6 defect), change in the local ply thickness and plies agglomeration which also was observed from the optical images obtained using a stereomicroscope (Carl Zeiss Stemi SV 11), shown in Figure 8. These discontinuities create local change in thickness that affects the reflected back wall signal causing higher signal attenuation.

Figure 9 C-scan amplitude maps for a focused UT signal along with the echo dynamics plots for different FOI in the glass fiber / PP specimen. A total of 5 scans were performed focusing at each individual embedded defect. Each scan was performed a cross the full specimen width in the X-direction; however, a distance of 42 mm where scanned across the sample length in the Y-direction. Figure 9a, shows that no enhancement was observed for the shape identification of the FOI A1 when compared to the results obtain in Figure 7. The FOI is located near to the back surface of the sample (~ 2.8 mm away from the specimen back surface) and the UT signal was highly attenuated. In order to reveal more details about the FOI A1, signal attenuation should be reduced. Scanning the part from the surface that is near to the FOI location and focusing the UT signal at the FOI depth would resolve the attenuation problem. On the other hand, Figure 9b shows enhancement in the shape detectability for defect A2. It was noticed that the area of the defect is more confined and less signal distortion was observed. The same trend was observed while scanning A3 and A4

FOI. Figure 9c provides an example of the advantage of using a focused PA UT system. It was noticed that when the signal was focused at 7.5 mm, the A3 FOI shape was identified; however, it is observed that the A5 FOI appears out of focus and its shape and size could not be detected, and the opposite trend was observed in Figure 9e. It was noticed that the FOI A5 (i.e. aluminum insert) was not detected when the UT signal was focused at the back wall. Figure 9e shows however that the shape of the FOI was recognized when the signal was focused at 4 mm beneath the specimen surface. The change in the local thickness caused by the fiber waviness at the top layers was captured. An increase for signal amplitude intensity for the fiber waviness areas was noticed when the signal was focused at the top plies of the specimens. The out of plane fiber waviness (i.e. along the thickness direction) was captured; however, the in plane waviness (i.e. X-Y direction) was not captured.

4.2.2 Through Transmission Ultrasonic

In order to reduce the attenuation of the UT signal, through transmission technique with lower frequency (i.e. 1 MHz) was used to scan the glass fiber / PP specimen. Figure 10 shows the amplitude C-scan through transmission UT results with a scanning frequency of 1MHz. It was observed that all of the FOI were captured and their shape and size were defined and analyzed. Figure 10 shows that the shape of the FOI was more defined when compared to the results obtained by the PA UT technique. The through transmission technique results in lower signal attenuation as it is strictly based on the amplitude of the received signal and not the attenuation of the back wall signal. However, information about the defect location across the sample thickness could not be obtained. The local change in the thickness created by out of plane fiber waviness was not captured (referred as II in Figure 7). Figure 10 showed that the texture of the composite (0º/90º) was captured due to the reduction in the signal distortion. The drawback of the TT UT technique is that the part needs to be accessible from both sides, which could not be practical in some cases.

5. DISCUSSIONS

The conventional X-ray system was only able to detect FOI as A3 and A5; however, all other defects were not detected. FOI such as A2 and A4 were made of Teflon that has a low X-ray attenuation coefficient

of ~ $1.632x10^{-01}$ cm^2/g [39] that resulted in low contrast differences between the defect and the background and made it hard for the radiography system to clearly identify these type of defects even when the micro focus tube was used. Kapton insert (i.e. A1) has a density of ~ 1.43 g/cm^3 [40] that resulted in measurable contrast differences when the CT X-ray system was used. The relatively low contrast difference between the Kapton insert and the background material was one of the reasons that made it difficult for the conventional X-ray system to detect this type of defect (i.e. the final image is a shadow image for the entire part thickness). Using a thin plane of inspection at the CT X-ray method (~ 0.35 mm) assisted in the elimination of any structural noise from the features outside this scanning plane and made the A1 FOI more visible. It should be noticed that, if a feature has a thickness of (***t***), however it was imaged with a slice of larger thickness of (***T***) (i.e. in case of conventional systems ***T*** will be equivalent to the full part thickness), the contrast would be reduced by a factor of ***t/T*** [33]. The contrast could be enhanced using low energy X-ray; however, it should be taken into consideration that this will result in high system noise that affects the detectability of the system. In contrast to the radiography systems, it was observed that the UT system detected all the FOI regardless of material.

Radiography techniques have an advantage over the ultrasonic methods when characterizing the defects' shape and size. The radiography results clearly show low distortion for the defect shape, as it is more like an optical image compared to the image obtained using the ultrasonic C-scan amplitude image. The shape of the FOIs was clearly defined. However, it was quite challenging to conduct an accurate size measurement for the embedded inserts using the 3-D reconstruction data obtained by the X-ray CT. MPR images (i.e. where oblique, front, side and top slices with finite thickness through the object are demonstrated) was used to perform dimensional analysis. Osirix imaging software was used to convert the 2-D images to MPR volumes, segmentation and visualization of the volumetric data set. There are some aspects that should be considered while analyzing the radiography images such as scattering, un-sharpness, uniformity in the gray scale values and metal artifacts that can cause problems and measurement inaccuracies. To overcome these problems image post processing was performed using Image J and Matlab software [41, 42]. FFT band-pass filter was applied then the images were then equalized, sharpened and the area of the required features (i.e. FOI size) was measured. Relative Error (RE) was used to estimate the precision of both of the radiography and UT

measurement,

$$e_{relative} = \frac{|D_{Scan} - D_{Actual}|}{D_{Actual}} \times 100 \quad (3)$$

where D_{Scan} and D_{Actual} are the scanned and actual area of the artificial embedded FOI. The scan results of each type of the FOI were compared with their actual size and the corresponding relative errors are listed in Table 2 and Figure 11. It was noticed that the radiography measurements do overvalue the actual size of the impeded defects, as the high coherence phase contrast resulted in an upward and downward overshooting of the gray values. The gray value overshooting was noticed at the edges of the FOIs and the polymer matrix and that was integrated in the FOI size measurement. Still the reported errors are relatively small as the maximum error for the measurements of the defects areas was below 9.5%. The overshooting for the gray values for the metallic FOI resulted from the artifact associated with the X-ray beam hardening. Image post processing assisted in decreasing the effect of the artifacts on the size measurement process. The relative error of 6.8% was reported for the CT X-ray measurement for the FOI A1 (i.e. Kapton insert) that has relatively low density when compared to metallic inserts or when compared to the background material. This is attributed to the fact that the system attempts to compensate the low contrast difference between the A1 and the background by overshooting the gray values for the defect to make it sharper for detection.

Unlike the radiography, the relative error for the ultrasonic measurements for the FOIs size was found to be relatively high (~ up to 75.4%). The PA UT system showed the highest relative error values among all of the NDE/T technique used in this research, as shown in Figure 11. It was noticed that the FOIs areas were surrounded with areas of relatively lower amplitude (~ 70 dB), shown in Figure 7, when compared to the amplitudes generated by the FOIs themselves. These areas of low amplitude were created due to the change of the local thickness or separation of the plies at the areas adjacent to the FOI areas. This was reflected on the defect size measurement resulting in high levels of relative error reported in Table 2. Furthermore, it was observed that the FOI created a bend of the composite plies below and above the embedded object, see Figure 12, which reflects on the measured values of the actual FOI area. In contradiction of the PA UT results, it was noticed that the values for the FOI areas were under estimated when through transmission UT system were used. The through transmission UT technique is based on the

attenuation of the amplitude of the received signal and not the attenuation of the reflected back wall signal (as in the PA UT system). The areas surrounding the FOI (i.e. areas of ply separation) produced an acoustic barrier preventing a portion of the ultrasonic signal from being transmitted through the FOI. It was noted that the area for the FOI A3 was overestimated. The inner area for the circular shape (i.e. Hollow inner part) is included in the measurement as it is shown in Figure 7 and Figure 10. The results obtained by the ultrasonic techniques can be enhanced using high frequency transducer that will help in revealing more details for the FOI. The drawback of using high frequency transducer is that smaller wavelength is generated which is rapidly attenuated, see Figure 6, and it can only travel through shorter distance. In a previous research a 5 MHz focused pulse-echo transducer and 5 MHz focused through transmission transducer were used to scan a glass fiber / PP sample and it was found that the signals were highly attenuated and none of the FOIs were detected [8].

Out-of-plane waviness in thick composite plates can be detected using ultrasonic Rayleigh wave produced by air coupled ultrasonic transducers [28]. In this research it was observed that the PA UT scans can provide information about out of plane fiber waviness, local change in thickness and ply agglomeration that could not be identified using through transmission technique or conventional X-ray system. The X-ray CT showed the ability to detect the out of plane and in plane fiber waviness (i.e. A6) in the specimen. The radiography methods and the UT through transmission method were able to identify the composite texture. However, it should be noticed that both of the conventional X-ray and UT through transmission systems provide fiber orientation only in 2-D plane and no information for the orientation through the part thickness could be obtained. The X-ray CT images could reveal level of detail down to the fiber distribution through the part depth. This could be obtained through high-resolution scans using CT-scanner with a microfocus X-ray tube [43]. Still, the technique suffers from sample size limitation. The specimen size should be less than 10 mm to resolve information about single fiber orientation [44]. In the PA UT method, the high signal attenuation and distortion affected the technique's ability to detect the fiber pattern in the composite specimen.

In order to evaluate the resulting image quality of the NDE techniques used in this work, the Contrast-to-Noise Ratio (CNR) values for different FOI detected were compared and listed in Table 3. The

mean pixel values and pixels standard deviation values for the gray color images were measured and used to calculate the CNR values according to [45, 46],

$$CNR = \frac{|M_O - M_B|}{\sqrt{0.5(\sigma_O^2 + \sigma_B^2)}} \quad (3)$$

where M_O is the mean pixel value of the FOI, M_B is the mean pixel value for neighboring background, σ_O is the standard deviation of pixel values of the FOI and σ_O is the standard deviation of pixel values of the neighboring background. Table 3 shows that all of the NDE techniques used provided good CNR values that made it easy to distinguish the FOI from the background material. The low CNR value (~ 0.81) for the aluminum insert (i.e. A5) when scanned using PA UT come in agreement with the results observed in Figure 7. The high signal distortion resulted in high levels of noise at the image and made it difficult to differentiate between the reflected signal and the background noise. The CNR results for the A1 FOI showed that the through transmission UT technique has an advantage over the other NDE technique in distinguishing the FOI from the background material. An improvement of 37.8% and 49.3% was observed when compared to the PA UT and X-ray CT scan respectively. The images resulted from the conventional X-ray showed increase in the CNR values for the FOI with high-density material (i.e. steel and aluminum inserts). For the A3 steel insert, a reduction of 40%, 41.4%, 9.1% in the CNR values for the X-ray CT scan, PA UT and TT UT respectively was observed when compared to the CNR values for the conventional X-ray.

In general, radiography technique has no need for couplant, provides high resolution, large field of view and good defect size and shape detectability. However, there are some disadvantage of the technique such as the mobility of the technique (i.e. the part should be disassembled and sent to the testing facility), the high initial and running cost of the CT scan systems, the required access to both sides of the part, shielding requirements, handling procedures and safety considerations as potential hazards associated with use of X-ray radiography. The ultrasonic techniques have the advantage of being portable (i.e. filed testing) with low safety hazards and law running cost. However, the part surface finish, porosity levels and the quality of coupling play a crucial rule in the interpretation of final results.

6. CONCLUSIONS

This paper has presented an investigation for different NDE/T methods for characterizing thermoplastic composites. The techniques were divided to two major groups: radiography methods and ultrasonic techniques. It was observed that the radiography methods have some limitations in identifying the FOIs with comparable density to the background material. The UT methods are successfully able to capture all of the FOI in the thermoplastic composite specimen regardless their material type. The shape of the defects is clearly visible when radiography methods are used; however, the shape of the defect is highly distorted when PA UT technique is applied. It was found that the distortion of the FOI shape will be reduced when 1 MHz through transmission UT are used. The size measurement for the FOI showed that the UT measurement has high relative error (up to 75.4%). In case of PA UT, this is due to interference of the echoes produced by the areas of ply separation adjacent to the FOIs area and the echoes produced by the FOI. However when through transmission UT was applied, theses area of separation form an acoustic barrier preventing a portion of the ultrasonic signal from being transmitted through the FOI resulting in under estimation for the area values. 2-D fiber texture was captured using X-ray radiography and through transmission UT; however, information about out of plane fiber waviness was not captured. X-ray CT is able to identify the fiber texture through the specimen depth and the out of plane fiber waviness was characterized. Table 4 summarizes the capabilities and limitation for the NDE/T methods used in this research to characterize different defects in glass fiber/ PP composite. This investigation suggests that a combination of different NDE/T techniques and prior knowledge with the characterization technique limitation would provide optimum results in identifying a range of defects and fully characterize glass reinforced thermoplastic composite parts.

7. ACKNOWLEDGEMENTS

All of the UT was performed using Marietta NDT Inc. facility at GA, USA. The authors would like to acknowledge the support and help of Ryan McCarthy and Daryle Higginbotham at Marietta NDT who made this research paper possible. The authors would like to acknowledge Professor Michael Yester at the Department of Radiology, University of Alabama at Birmingham for his efforts and support toward this research. Support from the Department of Energy Graduate Automotive Technology Education (DOE GATE)

is gratefully acknowledged.

8. REFERENCES

[1] Mazumdar S. What Will Drive Composites Growth in 2015? Composite Manufacturing. USA: American Composites Manufacturers Association (ACMA); January, 2015.
[2] Hambach M, Möller H, Neumann T, Volkmer D. Carbon fibre reinforced cement-based composites as smart floor heating materials. Composites Part B: Engineering. 2016;90:465-70.
[3] Ma H-l, Jia Z, Lau K-t, Leng J, Hui D. Impact properties of glass fiber/epoxy composites at cryogenic environment. Composites Part B: Engineering. 2016;92:210-7.
[4] Carrillo JG, Gamboa RA, Flores-Johnson EA, Gonzalez-Chi PI. Ballistic performance of thermoplastic composite laminates made from aramid woven fabric and polypropylene matrix. Polymer Testing. 2012;31(4):512-9.
[5] Xu LR, Krishnan A, Ning H, Vaidya U. A seawater tank approach to evaluate the dynamic failure and durability of E-glass/vinyl ester marine composites. Composites Part B: Engineering. 2012;43(5):2480-6.
[6] Mao ND, Thanh TD, Thuong NT, Grillet A-C, Kim NH, Lee JH. Enhanced mechanical and thermal properties of recycled ABS/nitrile rubber/nanofil N15 nanocomposites. Composites Part B: Engineering. 2016;93:280-8.
[7] Akonda MH, Lawrence CA, Weager BM. Recycled carbon fibre-reinforced polypropylene thermoplastic composites. Composites Part A: Applied Science and Manufacturing. 2012;43(1):79-86.
[8] Ahmed Arabi Hassen, Poudel A, Philip Chu T, Yester M, Vaidya UK. Tracing Defects in Glass Fiber/Polypropylene Composites Using Ultrasonic C-Scan and X-Ray Computed Tomography Methods. In: Testing ASfN, editor. ASNT Annual Conference. Charleston, SC, USA: ASNT; October, 2014.
[9] Poudel A, Shrestha SS, Sandhu JS, Chu TP, Pergantis CG. Comparison and analysis of Acoustography with other NDE techniques for foreign object inclusion detection in graphite epoxy composites. Composites Part B: Engineering. 2015;78:86-94.
[10] Dayal V. Wave propagation in a composite with a wavy sublamina. Journal of nondestructive evaluation. 1995;14(1):1-7
[11] Wu D, Steegmüller R, Karpen W, Busse G. Characterization of CFRP with Lockin Thermography. In: Thompson D, Chimenti D, editors. Review of Progress in Quantitative Nondestructive Evaluation: Springer US; 1995. p. 439-46.
[12] Munoz V, Valès B, Perrin M, Pastor ML, Welemane H, Cantarel A, et al. Damage detection in CFRP by coupling acoustic emission and infrared thermography. Composites Part B: Engineering. 2016;85:68-75.
[13] Chakrapani SK, Dayal V, Barnard D. Detection and characterization of waviness in unidirectional GFRP using Rayleigh wave air coupled ultrasonic testing (RAC-UT). Research in Nondestructive Evaluation. 2013;24(4):191-201
[14] Busse G, Wu D, Karpen W. Thermal Wave Imaging with Phase Sensitive Modulated Thermography. Journal of Applied Physics. 1992;71(8):3962-5.
[15] Palka N, Panowicz R, Chalimoniuk M, Beigang R. Non-destructive evaluation of puncture region in polyethylene composite by terahertz and X-ray radiation. Composites Part B: Engineering. 2016;92:315-25.
[16] Kastner J, Plank B, Requena G. Non-destructive characterisation of polymers and Alalloys by polychromatic cone-beam phase contrast tomography. Materials Characterization. 2012;64:79-87.
[17] Jones TS, Polansky D, Berger H. Radiation inspection methods for composite materials. NDT International. 1988;21(4):277-82.
[18] Ahmed Arabi Hassen, Vaidya UK, Frank Britt. Structural Integrity of Fiber Reinforced Plastic Piping. Material Evaluation. 2015;73(7):919-29.
[19] H. Hocheng, Tsao CC. Computerized Tomography and C-scan for Measuring Drilling-Induced Delamination in Composite Material Using Twist Drill and Core Drill. Key Engineering Materials. May, 2007;339:16-20.
[20] Goidescu C, Welemane H, Garnier C, Fazzini M, Brault R, Péronnet E, et al. Damage investigation in CFRP composites using full-field measurement techniques: Combination of digital image stereo-correlation, infrared thermography and X-ray tomography. Composites Part B: Engineering. 2013;48:95-105.

[21] Lowrey A. R, K. D Friddell, Cruikshank DW. Nondestructive Evaluation of Aerospace Composites Using Medical Computed Tomography (CT) Scanners. In: Proceedings of American Societyfor Nondestructive Testing (ASNT) Spring Conference. Washington, DC, USA, Conference, Conference 11-14 March, 1985.
[22] Zhen-Guo Y, B. L, J. S. Ultrasonic testing technique for small-calibre piping containing defects. International Journal of Pressure Vessels and Piping. 1996;68(3):325-30.
[23] Seshu D. Rama, Dakshina MNR. Non Destructive Testing of Bridge Pier - A Case Study. Procedia Engineering. 2013;54(0):564-72.
[24] Chakrapani SK, Dayal V, Barnard DJ. Investigation of waviness in wind turbine blades: Structural health monitoring. The 39th Annual Review of Progress in Quantitative Nondestructive Evaluation AIP Conf Proc of Progress in QNDE2013. p. 310-6.
[25] Green WH, Sincebaugh P. Nondestructive Evaluation of Complex Composites Using Advanced Computed Tomography (CT) Imaging. In: laboratory Ar, editor. Maryland, USAFeberuary, 2001.
[26] Theodoros H, Efstratios B, Nicolaos GT. Application of Ultrasonic C-Scan Techniques for Tracing Defects in Laminated Composite Materials. Journal of Mechanical Engineering. 2011;57(3):192-203.
[27] Chakrapani SK, Barnard D, Dayal V. Detection of in-plane fiber waviness in composite laminates using guided Lamb modes. AIP Publishing; 2014. p. 1134-40
[28] Chakrapani SK, Dayal V, Barnard DJ, Eldal A, Krafka R. Ultrasonic Rayleigh wave inspection of waviness in wind turbine blades: Experimental and finite element method. Review of Progress in Quantitative Nondestructive Evaluation AIP Conf Proc2012. p. 1911-7.
[29] Taheri H, Ladd KM, Delfanian F, Du J. Phased array ultrasonic technique parametric evaluation for composite materials. IMECE (ASME). Montreal, Canada,November, 2014.
[30] Hopkins D, Neau G, Ber LL. Advanced Phased-Array Technologies For Ultrasonic Inspection of Complex Composite Parts. Smart Materials, Structures & NDT in Aerospace Conference. Montreal, Quebec, CanadaNovember 2011.
[31] Rosset A SL, Ratib O. OsiriX: an open-source software for navigating in multidimensional DICOM images. Journal of Digit Imaging. Sep 2004;17(3):205-16.
[32] ASTM. Standard Method for Verifying the Alignment of X-ray Diffraction Instrumentation for Residual Stress Measurement. E915, Vol301,. USA: ASTM; 1986.
[33] ASTM. Standard Guide for Computed Tomography (CT) Imaging. ASTM E1441-11. USA: ASTM; 2011.
[34] Oster R. Computed Tomography as a Non-destructive Test Method for Fiber Main RotorBlades in Development, Series and Maintenance. In: Proceedings of International Symposium on Computerized Tomography for Industrial Applications and Image Processing in Radiology. Berlin, Germany, Conference, Conference March, 1999.
[35] Peter E, Skaug Sande, Catrine A, Trægde Martinsen, Hole EO, Olerud HM. Interphantom and interscanner variations for Hounsfield units—establishment of reference values for HU in a commercial QA phantom. Physics in medicine and biology. 2010;55:5123-35.
[36] Mallick PK. Fiber reinforced composites: Materials, Manufacturing, and Design. New York, USA: Taylor and Francis Group; 2008.
[37] Boas FE, Fleischmann D. CT artifacts: Causes and reduction techniques. Imaging in Medicine. 2012;4(2):229-40.
[38] De Man B., Nuyts J, Dupont P, Marchal G, Suetens P. Metal streak artifacts in X-ray computed tomography: a simulation study. IEEE Transactions on Nuclear Science. 1999;46(3):691-6.
[39] Hubbell JH, Seltzer SM. Tables of X-ray mass attenuation coefficients and mass energy-absorption coefficients 1 keV to 20 MeV for elements Z= 1 to 92 and 48 additional substances of dosimetric interest. National Inst. of Standards and Technology-PL, Gaithersburg, MD (United States). Ionizing Radiation Div.; 1995.
[40] DuPontTM Kapton® HN. Polyimide film: Technical Data Sheet. In: DuPont, editor.2011.
[41] Tiago Ferreira, Wayne Rasband. ImageJ User Guide. In: Health NIo, editor. USA: National Institutes of Health; October, 2012.
[42] MathWorks. Matlab Primer R2014a manual. MA, USA: Mathwork, Inc.; 2014.
[43] Sutcliffe MPF, Lemanski SL, Scott AE. Measurement of fibre waviness in industrial composite components. Composites Science and Technology. 2012;72(16):2016-23.

[44] Revol V, Plank B, Kaufmann R, Kastner J, Kottler C, Neels A. Laminate fibre structure characterisation of carbon fibre-reinforced polymers by X-ray scatter dark field imaging with a grating interferometer. NDT & E International. 2013;58:64-71.
[45] Muhogora W, Devetti A, Padovani R, Msaki P, Bonutti F. Application of European protocol in the evaluation of contrast-to-noise ratio and mean glandular dose for two digital mammography systems. Radiat Prot Dosim. 2008;129(6):129-231.
[46] Muhogora W, Padovani R, Msaki P. Initial quality performance results using a phantom to simulate chest computed radiography. Journal of Medical Physics. 2011;36(1):22-8.

Table(s)

Tables

Table 1: Artificial defects location, size and material for glass fiber/PP panel

Defect #	Shape	Area (mm^2)	Thickness (mm)	Location in Z-direction	Defect Material
A1	Square	105.2	0.15	Between ply No. 14 and 15	Kapton
A2	Square	104.1	0.12	Between ply No. 34 and 35	Teflon
A3	Circle	172.7	2	Between ply No. 40 and 41	Steel sheet
A4	Triangle	107.8	0.12	Between ply No. 48 and 49	Teflon
A5	Square	349.1	0.6	Between ply No. 60 and 61	Aluminum sheet
A6	Fiber-waviness	N/A	N/A	Oversize cut of ply No. 68 to 80	-

Table 2: Defect size measurements and RE associated with the characterization techniques for the glass fiber/PP specimen

Defect #	Shape	Size (mm^2)					RE (%)			
		Actual	X-ray	CT-scan	PA UT	TT UT	X-ray	CT-scan	PA UT	TT UT
A1	Square	105.2	-	112.38	136.4	82	-	6.8	29.6	22
A2	Square	104.1	-	-	158.4	79.1	-	-	52.1	24
A3	Circle	172.7	187.3	173.7	302.9	290.7	8.4	0.54	75.4	68.3
A4	Triangle	107.8	-	-	176.2	75.3	-	-	63.4	30.1
A5	Square	349.1	354.7	382.2	503.2	437.7	1.6	9.5	44.1	25.4

Table 3: Contrast-to-Noise Ratio (CNR) average values for the FOI in the glass fiber / PP specimen

Defect #	Defect Material	CNR			
		Conventional X-ray	X-ray CT-scan	PA UT	TT UT
A1	Kapton	-	1.37	1.68	2.7
A2	Teflon	-	-	1.74	2.91
A3	Steel plate	3.5	2.1	2.05	3.18
A4	Teflon	-	-	1.54	2.1
A5	Aluminum sheet	13.9	10.5	0.81	7.5

Table 4: Capabilities and limitations for the UT and radiography methods used for characterizing the glass fiber/ PP composite

		NDE/T characterization method			
		Conventional X-ray	**X-ray CT-scan**	**PA UT**	**TT UT**
Fiber texture	2-D	X	X		X
	3-D		X		
Fiber waviness			X	X	
FOI with comparable density				X	X
Through the thickness detection			X	X	
Accurate FOI shape detection		X	X		X
Accurate FOI size detection		X	X		
In field inspection				X	X
Single sided scan				X	

Figure(s)

Figuers

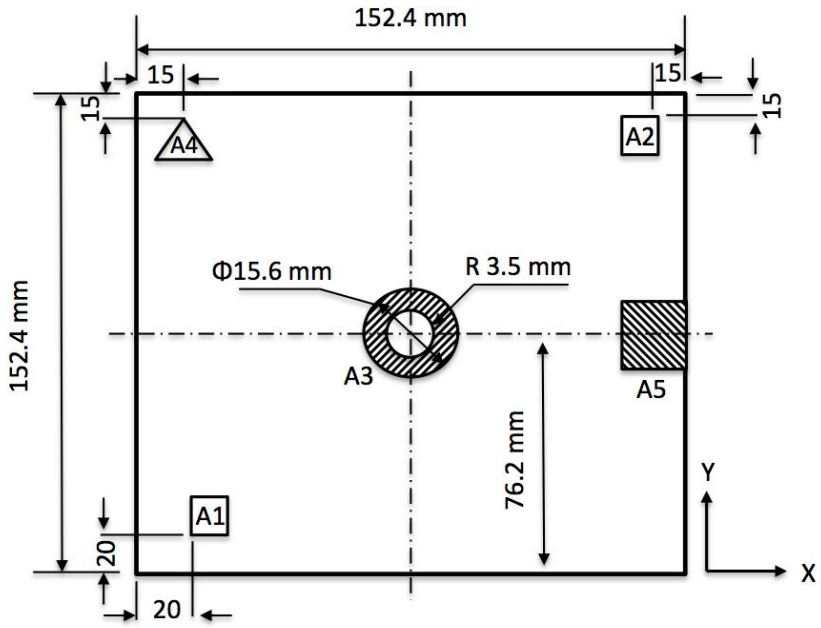

Figure 1: Schematic for defects location in glass fiber / PP panel

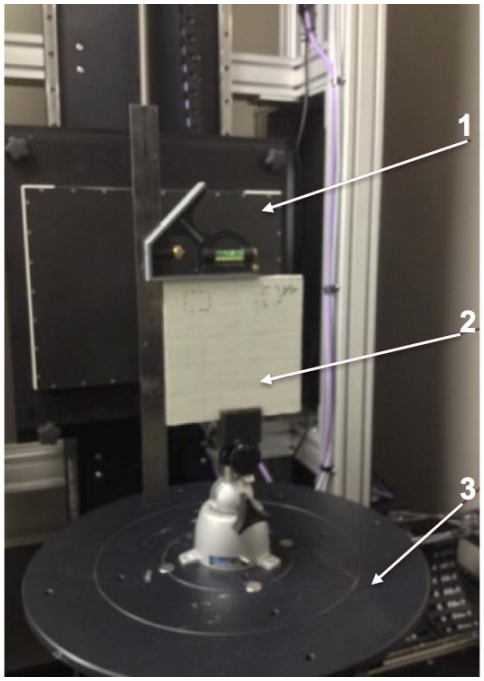

Figure 2: Test setup for X-ray imaging for glass fiber/PP specimen, 1) X-ray detector, 2) Composite specimen, and 3) Positioning table

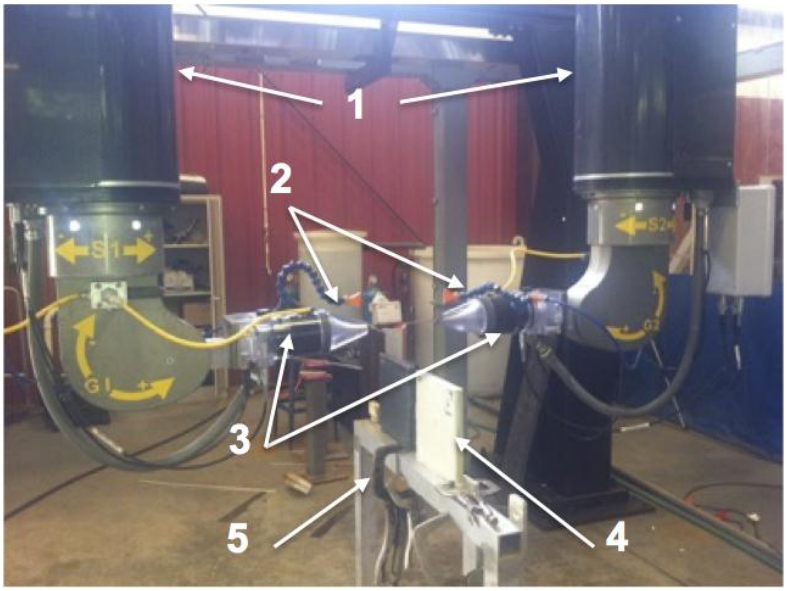

Figure 3: AG-2 overhead scanner system, 1) Robot arms, 2) Water nozzles, 3) 1MHz ultrasonic transducers, 4) Composite specimens and 5) Holder and specimen clamping device

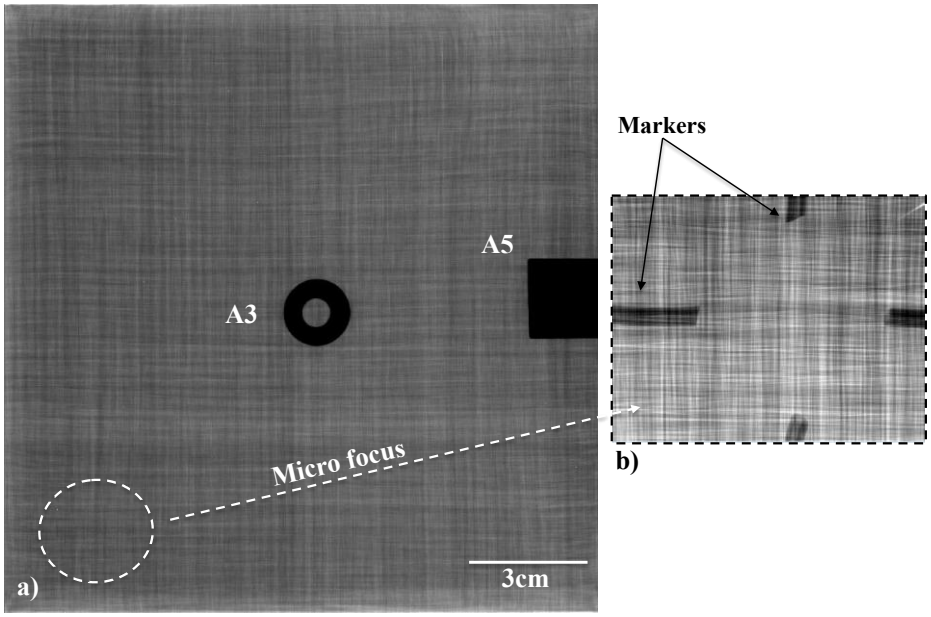

Figure 4: X-ray results for the glass fiber/ PP specimen, a) Scan for the full specimen area showing A3 and A5 FOI, and b) Micro-focus image in attempt to find FOI A1 (Kapton)

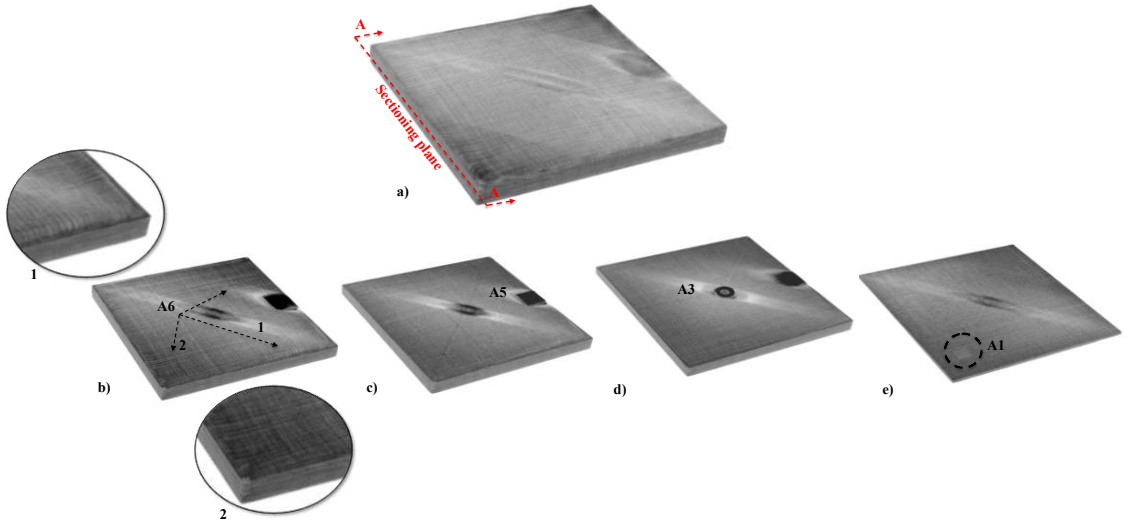

Figure 5: X-ray CT scan volume reconstruction for the glass fiber/ PP specimen, a) Complete part reconstruction showing the sectioning plan direction of A-A, b) Section at 1.5 mm showing fiber waviness at different locations; b1) & b2) Magnified images for the fiber wash areas, c) Section at 4 mm showing the aluminum plate insert, d) Section at 7.5 mm showing thesSteel plate insert, e) Section at 11.5 mm showing the Kapton insert

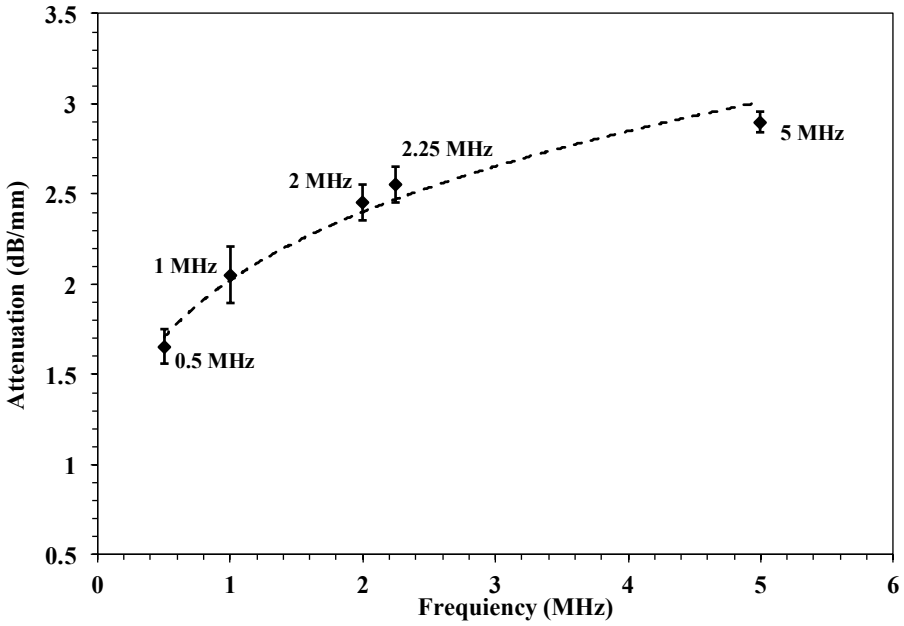

Figure 6: Attenuation coefficient as a function of the frequency for glass fiber / PP composite specimen

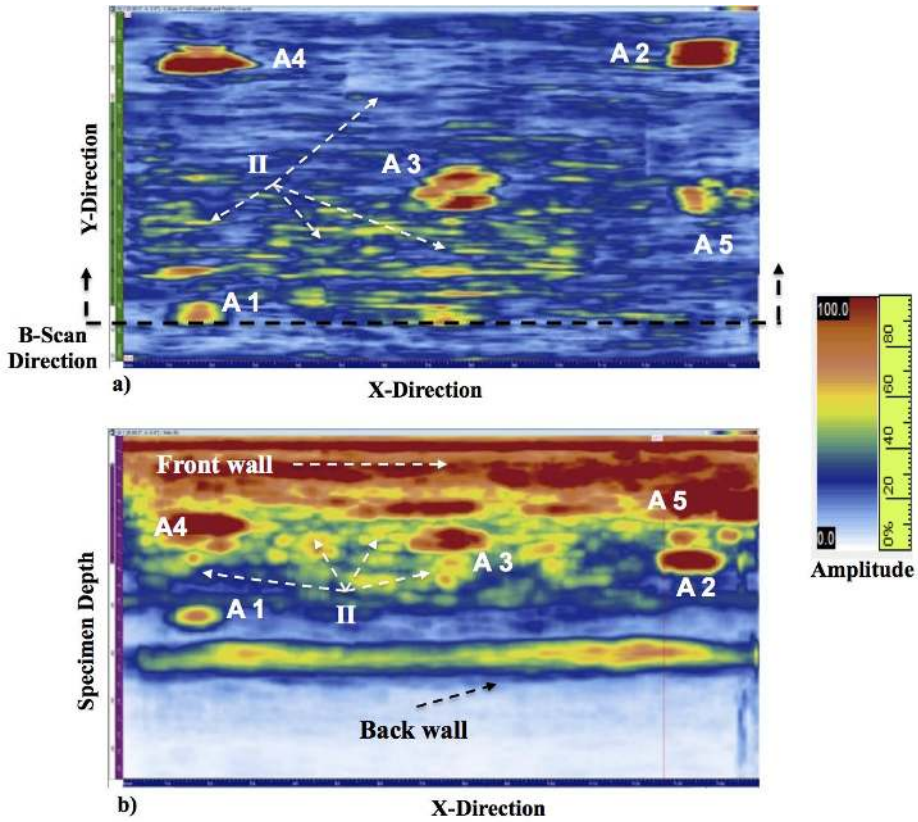

Figure 7: PA UT results for glass fiber/PP specimen gate was placed at the back wall echo; a) Amplitude C-scan map at 2.25 MHz, b) Amplitude B-scan map at 2.25 MHz; II) Areas represents the existence of fiber waviness and local change in the ply thickness

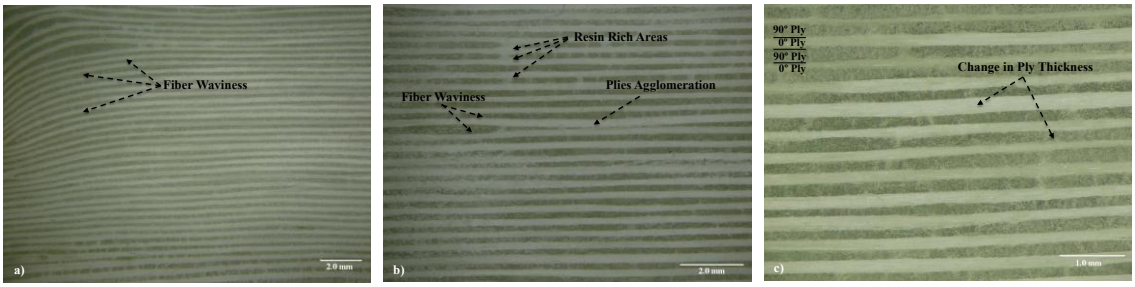

Figure 8: Stereography images for the glass fiber / PP specimen at location II in Figure 7; a) Areas of fiber waviness, b) Areas showing ply agglomeration, fiber waviness and resin rich areas; and c) Local change in the ply thickness

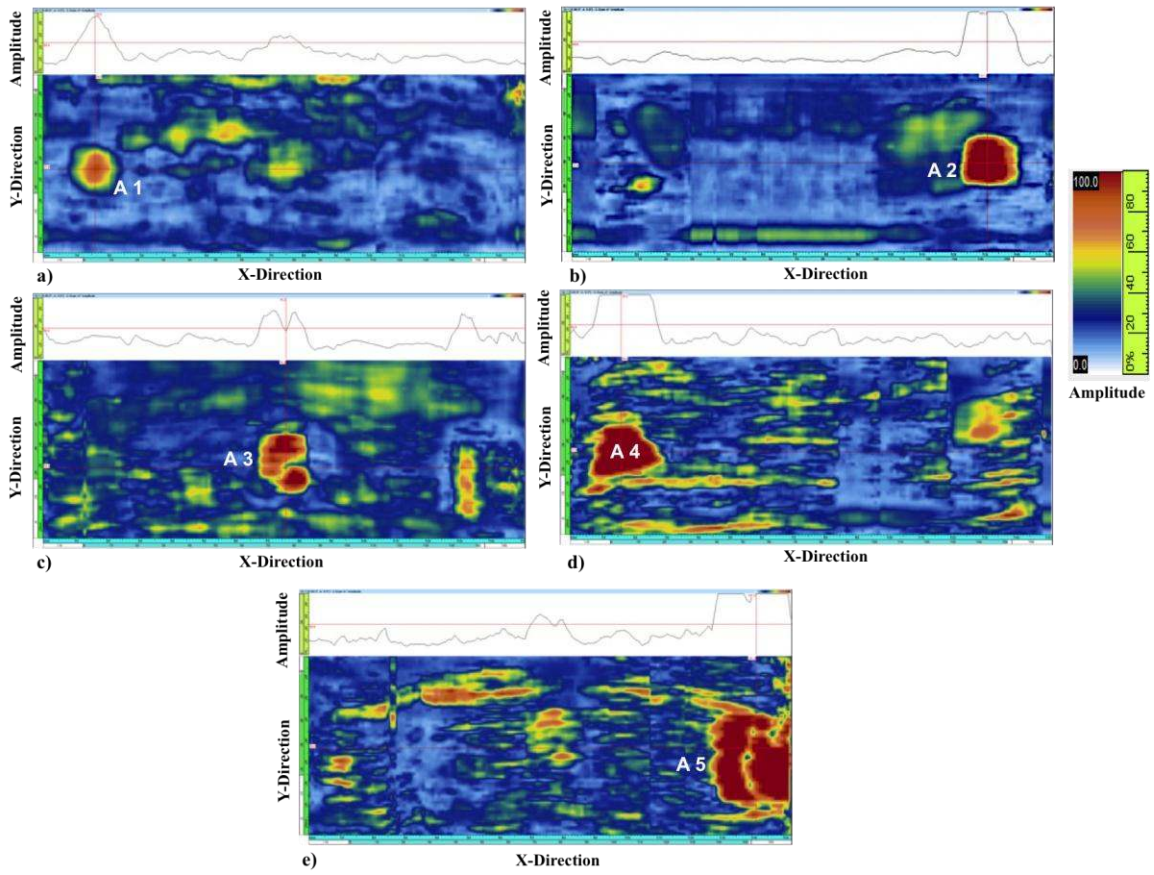

Figure 9: C-scan amplitude map for the defects using PA focusing method, a) Signal focused at 11.5 mm showing the Kapton insert (A1), b) Signal focused at 9 mm showing the Teflon insert (A2), c) Signal focused at 7.5 cm showing the steel insert (A3), d) Signal focused at 6.5 mm showing the triangle shape Teflon insert (A4), and e) Signal focused at 4 mm showing the Aluminum plate insert (A5)

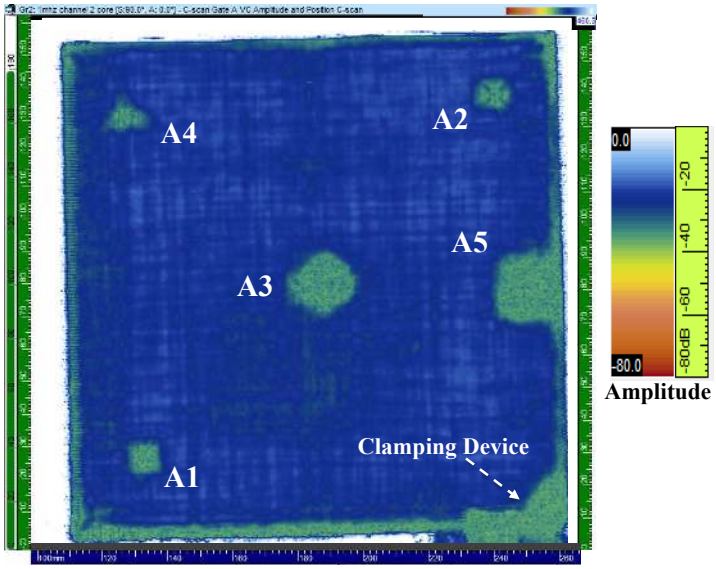

Figure 10: Through transmission C-scan amplitude map for the glass fiber/PP specimen showing the location for the FOI

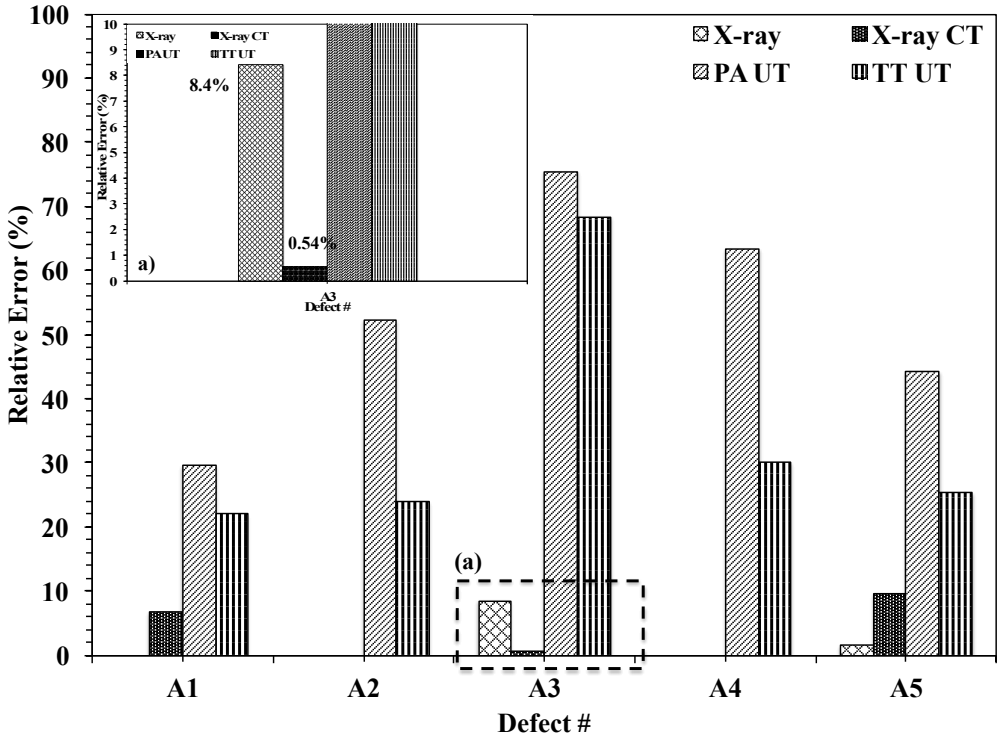

Figure 11: Relative error accompanying with the NDE/T techniques for different FOI; a) Extend scale showing error values for FOI A3

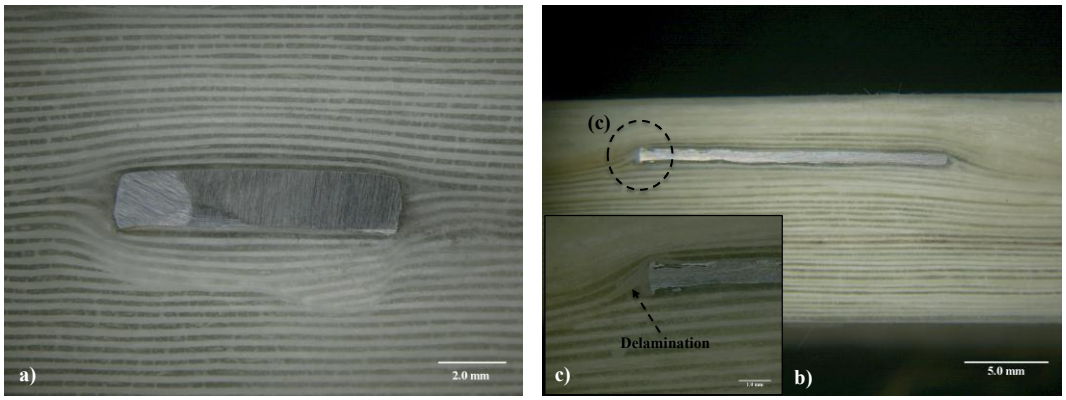

Figure 12: Stereography graphs for the glass fiber/ PP specimen showing bending of the composite plies below and above the defect, a) Steel insert (A3), d) Aluminum plate insert (A5), and c) Magnified image showing delaminated areas